NANO LETTERS

pubs.acs.org/NanoLett

Letter

Growth Rate and Thermal Properties of DNA Origami Filaments

Lena J. Stenke and Barbara Saccà*

Cite This: *Nano Lett.* 2022, 22, 8818−8826

Read Online

ACCESS | Metrics & More | Article Recommendations | Supporting Information

ABSTRACT: Synthetic DNA filaments exploit the programmability of the individual units and their predictable self-association to mimic the structural and dynamic features of natural protein filaments. Among them, DNA origami filamentous structures are of particular interest, due to the versatility of morphologies, mechanical properties, and functionalities attainable. We here explore the thermodynamic and kinetic properties of linear structures grown from a ditopic DNA origami unit, i.e., a monomer with two distinct interfaces, and employ either base-hybridization or base-stacking interactions to trigger the dimerization and polymerization process. By observing the temporal evolution of the system toward equilibrium, we reveal kinetic aspects of filament growth that cannot be easily captured by postassembly studies. Our work thus provides insights into the thermodynamics and kinetics of hierarchical DNA origami assembly and shows how it can be mastered by the anisotropy of the building unit and its self-association mode.

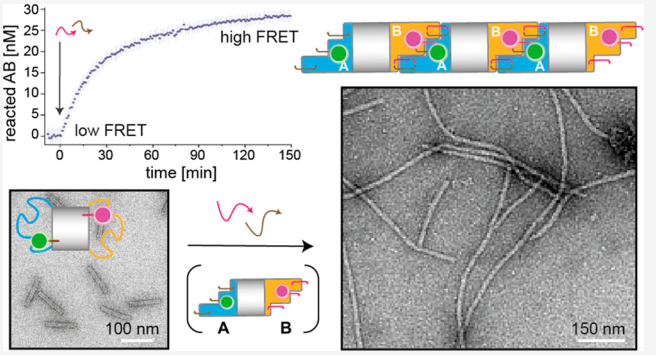

KEYWORDS: *DNA origami, hierarchical assembly, filament growth, hysteresis, FRET*

Protein filaments are key to many cellular functions since their dysregulation often leads to the occurrence of disease states.[1−6] The structural and dynamic properties of protein filaments are encoded in the building units, periodically repeated along the polymer chain. Several mechanisms have been postulated to explain these features[7−9] and many of the proposed models have served as theoretical frameworks for the rational design of synthetic polymers.[10−13] Nowadays, general construction principles and sophisticated chemical methods are available to control not only the length distribution and growth rate of filamentous structures, but also the kinetic route to otherwise inaccessible metastable assemblies.[14−16]

A successful approach for the realization of synthetic filaments relies on the use of DNA tiles.[17] These small intertwined motifs are equipped with short single-stranded extensions, whose programmable hybridization dictates the association rate and strength of tile-to-tile binding[18−24] and obeys a nucleation-and-growth mechanism.[25−28] Recent findings have shown that large DNA architectures, such as DNA origami, can be advantageously employed as nucleation seeds for the assisted growth of DNA-tile assemblies.[28−30] Conversely, the use of DNA origami structures as building elements of synthetic filaments has been so far mainly limited to the structural characterization of the end products.[31−41] Only few recent studies have focused on the programmable valency of DNA origami patchy particles as a means to control the degree of monomer hybridization into polymers,[37−43] whereas, to the best of our knowledge, no reports have yet addressed the different impact of base-stacking and base-hybridization on the temporal evolution of these structures. More efforts in this direction are motivated by at least two features of origami structures that are absent in DNA tiles, namely, (i) a high number of interactions per monomeric unit and (ii) shape-complementarity rules of interunit recognition. The former favors the multivalent and cooperative binding of origami units into hierarchical structures,[37,40] the latter provides a unique mechanism of self-association that solely relies on the geometry of the building block.[34,44,45] These properties, together with the versatility of sizes and shapes, and the modularity of assembly strategies, make DNA origami filaments appealing materials with a large spectrum of morphologies, mechanical properties, and chemical functionalizations attainable.

In this work, we provide a model system for the hierarchical and modular assembly of DNA origami units into linear filaments and investigate in detail the comparative effect of base-hybridization and base-stacking on the thermal stability and kinetic properties of the assemblies. To achieve our goal, we use a ditopic DNA origami monomer, i.e., a building block that—in its active state—features two terminal tips differing both in sequence and shape.[36] This two-fold anisotropy offers

Received: June 4, 2022
Revised: October 14, 2022
Published: November 3, 2022

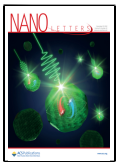

https://doi.org/10.1021/acs.nanolett.2c02255
Nano Lett. 2022, 22, 8818−8826

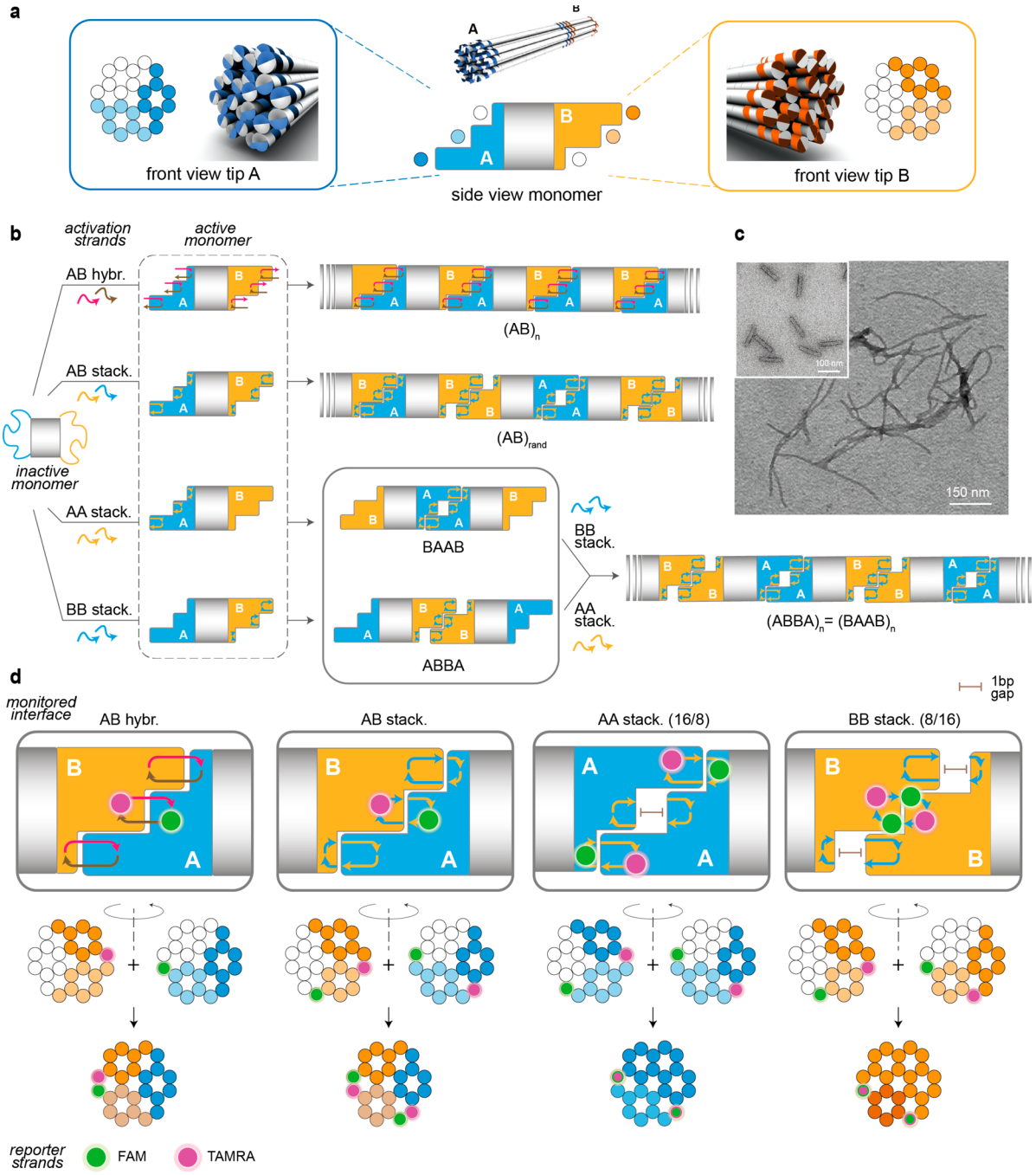

Figure 1. Design of the AB monomer and FRET labeling strategy. (a) The AB unit is a 24-helix bundle composed of three patches of eight helices each and displays both sequence and shape anisotropy. Each patch is indicated in color-code (A in blue and B in orange, with increasingly darker colors indicating a higher extent of helical protrusions). (b) The inactive monomer can be activated by hybridization (red and brown) or stacking (yellow and blue) strands to promote its self-association into linear oligomers of defined or random polarity (respectively indicated as $(AB)_n$ and $(AB)_{rand}$). Ordered stacked oligomers, $(ABBA)_n$ or $(BAAB)_n$, result from the stepwise association of preformed stacked dimers. (c) TEM imaging of equilibrium structures, before (inset) and after polymerization, demonstrate the successful implementation of the assembly strategy (here, an exemplary image of $(AB)_n$ filaments). (d) Top panels: A and B tips were labeled with one or two pair(s) of fluorescent dyes (FAM and TAMRA, indicated by green and magenta circles) to enable the monitoring of monomer association at heterologous (AB) or isologous (AA or BB) interfaces (details of the labeling strategy are reported in Figure S2). Bottom panels: Front views of the three patches are indicated in color-code for each monomer interface and interacting mode. The contacts established between the two monomer tips are indicated in the merged patches (last row) obtained by assuming to observe the construct along the central axis and from the left side (increasing color depth indicates increasing extent of helical protrusions).

two modes of molecular recognition (base-hybridization and base-stacking) that can be specifically harnessed to guide monomer association. In our previous work, we reported the consequence of this approach on the structural and elastic features of the resulting polymers.[36] Here, we show the impact of this strategy on the thermodynamic and kinetic features of the polymerization reaction and reveal energetic aspects of the process that cannot be easily disclosed by observation of the

https://doi.org/10.1021/acs.nanolett.2c02255
Nano Lett. 2022, 22, 8818−8826

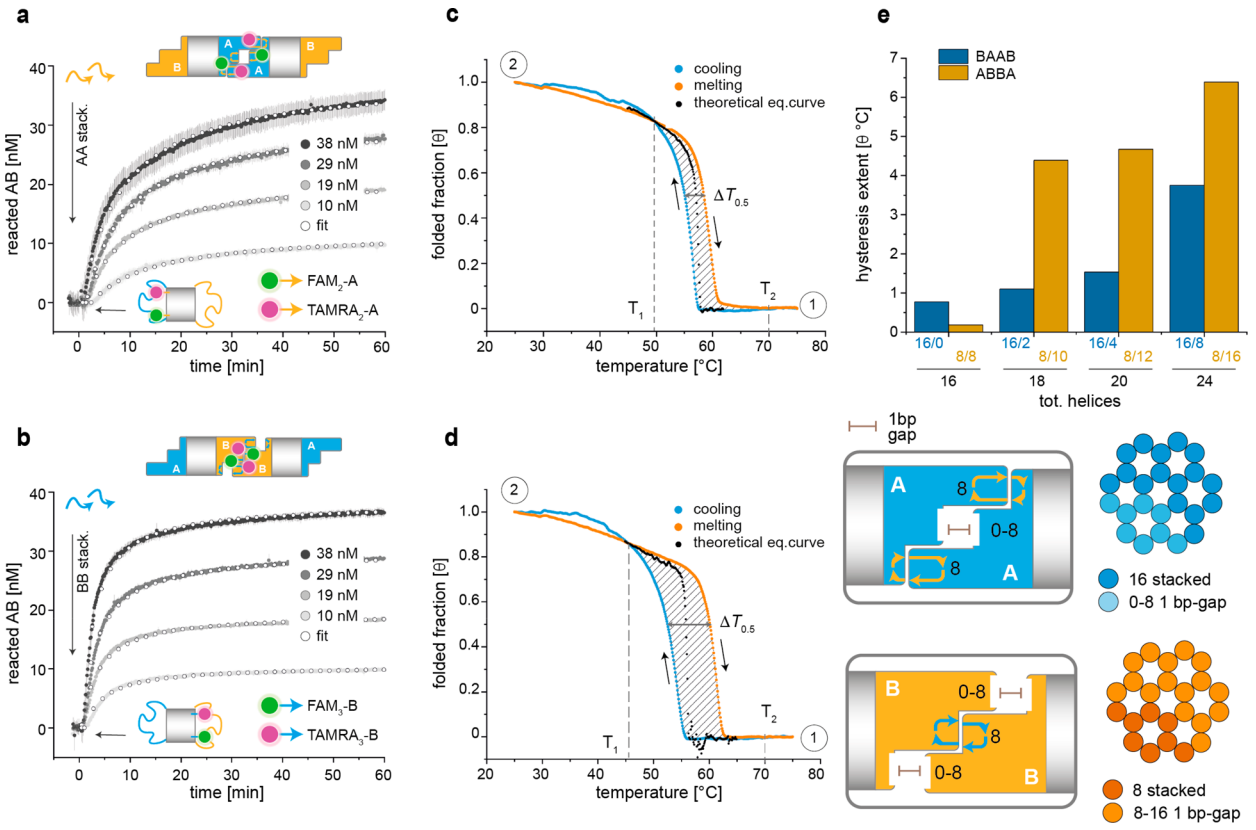

Figure 2. Kinetic and thermal characterization of dimer assembly. Isologous stacking at the AA (a) or BB (b) interface was monitored over time by FRET, upon addition of the corresponding stacking strands at 30 °C and different initial concentrations of inactive monomer (from about 10 to 40 nM) labeled with FAM/TAMRA reporter strands. The same FRET-labeling strategy was applied in thermal experiments to monitor the one-step assembly and disassembly of the dimer (blue and orange profiles, respectively) when stacked at the AA (c) or BB (d) interface. Thermal cycle: from 75 °C (point 1) to 25 °C (point 2) at −0.1 °C/min and reverse (from 2 to 1 at the same rate). The hysteresis of the thermal processes (shaded areas between the thermal curves) takes place between a defined interval of temperatures (T_1 and T_2). The theoretical equilibrium curve (black line) was reconstructed as described in SI Note 2. (e) Additional temperature-dependent FRET experiments were performed on dimers with a constant number of perfectly stacked helices and a variable number of 1-bp gapped helices (indicated as stacked/gapped helices: 16/0 to 16/8 for BAAB and 8/8 to 8/16 for ABBA, color-codes as in Figure 1; more details are in Figures S10−S13).

products at equilibrium. Hence, our data can help to rationalize the design of hierarchical DNA origami structures and improve control of the assembly process, providing a valuable tool for the advancement of DNA-based materials.

Design of the DNA Origami Monomer. The monomeric unit of our linear polymers is a DNA origami bundle of 24 helices, organized into three patches of 8 helices each (Figure 1a and Figure S1).[36] The structure is 102 nm long, has a diameter of about 18 nm and its terminal tips, herein called A and B, are mutually complementary and partially self-complementary in shape. Referring to A and B, respectively, as the head and tail of the monomer, we can distinguish three modes of monomer association: head-to-tail (AB), head-to-head (AA), and tail-to-tail (BB). Each mode of interaction is triggered by the addition of activation strands to a preassembled inactive monomer (Figure 1b). Correspondingly, three types of filaments can be constructed, namely, $(AB)_n$, $(AB)_{rand}$ and $(ABBA)_n = (BAAB)_n$. The first type of filament results from activation of the base-hybridization pathway. This promotes the binding of the A tip of one monomer to the B tip of a second monomer, leading to perfect match of monomer tips and formation of a linear structure of defined polarity and periodic sequence, $(AB)_n$ (Figure 1b, top panel). Activation of the stacking pathway at the A and B tips simultaneously yields the $(AB)_{rand}$ filament, characterized by the random association of monomers at all three possible interfaces (Figure 1b, middle panel). Finally, stepwise addition of stacking strands to preassembled BAAB or ABBA dimers enables the controlled extension of dimeric units in opposite directions and results in the formation of periodic filaments of identical sequence, $(ABBA)_n = (BAAB)_n$ but distinct assembly histories (Figure 1b, bottom panel). Hence, activation strands provide the monomer with the molecular information for growing at its ends, resulting into filaments of different periodicity and polarity.

Monitoring Tip Association through FRET. To characterize the rate of monomer association, we developed the FRET assay illustrated in Figure 1d. For each monomer tip, we selected one or two strands (referred to as reporter strands) and labeled their termini with a fluorescein (FAM) or a rhodamine (TAMRA) dye to monitor every mode of interaction by FRET (Figure S2). We recorded the rate of dimer or polymer formation at a given temperature, immediately after addition of hybridization or stacking strands to a solution of inactive monomer. Additionally, temperature-dependent FRET spectroscopy was applied to dimers or preassembled polymers to gain insights into the thermal stability of interunit binding and its impact on the hysteresis of the assembly/disassembly process.

https://doi.org/10.1021/acs.nanolett.2c02255
Nano Lett. 2022, 22, 8818−8826

Association Kinetics and Thermal Stability of Stacked Dimers. The inactive monomer was labeled with reporter strands and treated with excess stacking strands to promote binding either at the AA or BB interface. This allowed to monitor the extent of monomer consumption over time and its full conversion into the corresponding dimer (progress curves for different initial monomer concentrations, from 10 to 40 nM, are shown in Figure 2a,b). The initial rates in the linear phases of the curves were used to extract the apparent association rate coefficient of the process (k_a^{in}, Table 1, Figure S3 and SI Note 1). The data indicate that, at 30 °C, stacking at the B tips is about 2-fold faster than stacking at the A tips, with an association rate coefficient of about $(14.4 \pm 0.1)10^{-2}$ min^{-1} and $(30 \pm 4)10^{-2}$ min^{-1} for the BAAB and ABBA dimer, respectively. The total and irreversible formation of the dimers was proven by agarose gel electrophoresis (AGE) and atomic force microscopy (AFM) and for both dimers, the initial rate of dimerization increased with the temperature, as expected (Figures S4 and S5).

Table 1. Thermal and Kinetic Parameters of Origami Dimer Formation and Dissociation

dimer	temp. scan	$T_{0.5}$ [a] [°C]	T_m [b] [°C]	T_{th} [c] [°C]	A [d] [θ °C]	k_a^{in} [10^{-2} min^{-1}] [e]
BAAB	heat	58.5	59.8	57.6	7.08	14.4 ± 0.1
	cool	55.1	56.7		4.18	
	Δ	3.4	3.1		2.90	
ABBA	heat	60.1	61.4	55.8	12.4	30 ± 4
	cool	52.5	54.2		6.38	
	Δ	7.6	7.2		6.03	

[a]Temperature at $\theta = 0.5$. [b]Temperature at $d^2\theta/dT^2 = 0$. [c]Theoretical temperature for a simulated equilibrium curve (Suppl. Note 2). [d]Area (A) included between the heating (or cooling) profile and the temperature axis. Δindicates the difference between the values of temperature or area associated with the heating and cooling profile. [e]Values obtained from isothermal FRET experiments at 30 °C.

A plausible explanation for the different association rates relies on the structural features of the monomer at the two terminal tips. As stated above, the A and B edges of the monomer are designed to be mutually complementary in shape: the three helical patches of A perfectly match with the corresponding three helical patches of B, building a bundle of 24 continuous duplexes (Figure 1d, panel I and II). On the contrary, isologous stacking results from the partial shape-complementarity of edges of the same type, yielding a bundle with a defined number of 1-bp gaps in between the monomers. Specifically, stacking of two monomers at their A interfaces results in two pairs of stacked patches (2 × 8 helices), with the third pair of 8 helices separated by 1-bp gap; this construct is indicated as 16/8 (Figure 1d, panel III). Conversely, BB stacking entails one pair of stacked patches and two pairs of patches separated by 1-bp gap (8/16 in Figure 1d, panel IV). BB stacking is therefore sterically less demanding, structurally more flexible, and presumably easier to achieve, explaining the higher rate of ABBA dimer formation as compared to the BAAB dimer.

We then investigated the thermal properties of the stacked dimers by temperature-dependent FRET spectroscopy. In these experiments, one-pot assembly and disassembly of the structures was performed on a mixture of oligonucleotides that included all sequences needed for formation of the inactive monomer, as well as the stacking and reporter strands (Figure 2c,d, for the BAAB and ABBA dimer, respectively). Control AGE and AFM studies confirmed correct formation of the dimers according to this procedure (Figures S6 and S7). The data indicate that the thermal transitions are cooperative but nonreversible, with BAAB displaying a lower extent of hysteresis than ABBA (Table 1).

The appearance of hysteresis in the thermal assembly and disassembly of DNA origami structures is a known phenomenon,[46] typically attributed to the complexity and diversity of paths that can be traveled by the system to reach the final fold and then melt the intricate structure. This deviation from thermal reversibility is proportional to the area between the melting and cooling profiles (shaded areas in Figure 2c,d).[47] Accordingly, stacking and melting of the BB interface dissipates almost 2-fold the energy involved in a folding/unfolding cycle at the AA interface and is thus further from a condition of pseudoequilibrium (Table 1, SI Note 2, Figures S8 and S9). We then examined whether the helical gaps at partially stacked monomer interfaces may affect the thermal behavior observed and analyzed various dimeric constructs that differed only in the number of such gaps (constructs 16/0 to 16/8 for BAAB and 8/0 to 8/16 for ABBA, Figure 2e and Figures S10−S13). The results show that the T_m (for both the cooling and heating profiles), as well as the hysteresis of one thermal cycle, scale with the number of 1-bp gaps; however, in a sequence-dependent manner. When compared to the AA interface, the presence of helical gaps at the BB interface has a larger impact on the thermal stability of the structure, although a higher number of gaps is required to show an appreciable extent of hysteresis (cfr. 16/8 for the BAAB and 8/10 for the ABBA in Figure 2e). We deduce that sequence-dependent structural distortions at the blunt ends of gapped helices may allow for short-range interactions that, by restoring helical stacking to some degree, essentially reduce the size of the cavity. This is in agreement with previous studies on nicked DNA duplexes[48,49] and may explain the hysteresis phenomenon as a consequence of distorted helical configurations at the interface of two monomers. Altogether, these data indicate that the thermal and kinetic features of stacked DNA origami dimers can be programmed by both the nucleobase composition and geometry of the monomer tips, with helical gaps extending the level of control attainable.

Kinetics of Filament Formation. We then applied the FRET strategy described above to gain quantitative information on the rate of monomer (or dimer) incorporation into different types of DNA origami filaments (Figure 3 and Figures S14−S20). We developed seven distinct FRET assays. Three assays enabled to record the formation of the periodic filaments, namely, the head-to-tail hybridization of AB monomers (Figure 3a), the head-to-head stacking of preformed ABBA dimers and the tail-to-tail stacking of preformed BAAB dimers. For the random constructs, we prepared one type of filament where all stacked associations were visible (rand_all) and three types of filaments in which only selected pairs of stacking contributions could be monitored, although all were present (rand_AB, rand_AA and rand_BB; Figure 3b for rand_AB).

Isothermal experiments were carried out at different initial monomer concentrations (between 5 and 35 nM) and three temperatures (30, 35, and 40 °C) were analyzed to estimate the energy barrier of the reaction (Figure 3c,d). The initial linear phase of the FRET traces was used to extract the apparent association rate coefficient of the reaction (Table 2).

https://doi.org/10.1021/acs.nanolett.2c02255
Nano Lett. 2022, 22, 8818−8826

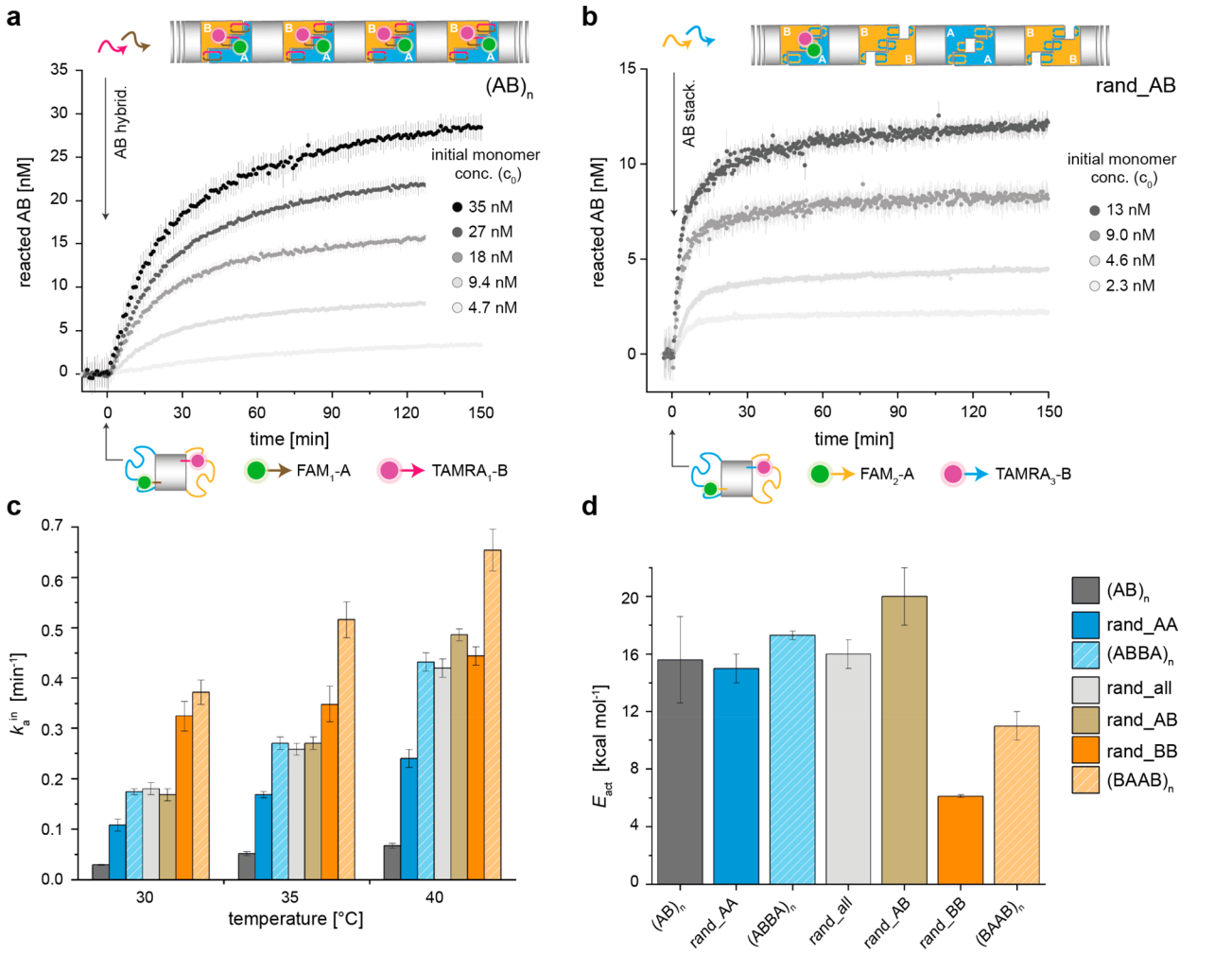

Figure 3. Kinetics of DNA origami filament growth (I). The FRET strategy reported in Figure 1d was used to monitor the self-association of the monomer into three types of filaments. Representative curves are given for the head-to-tail association of the monomer into (a) the periodic $(AB)_n$ filament and (b) the random filament (rand_AB), at 30 °C, and for different initial concentrations of the monomer. (c) Application of the FRET strategy to all possible filaments and monomer interfaces enabled to extract the values of the association rate coefficients (k_a^{in}) for the initial phase of the reaction. (d) The dependence of these values from the temperature was finally used to calculate the activation energies (E_{act}) of the polymerization reactions.

Table 2. Association Rate Coefficients (k_a^{in} in min^{-1}) and Activation Energies (E_{act} in kcal mol^{-1}) Referred to the Initial Linear Phase of DNA Origami Filament Formation

T [°C]	$(AB)_n$ hybr	rand_AA	$(ABBA)_n$	rand_all	rand_AB	rand_BB	$(BAAB)_n$
30	0.029 ± 0.001	0.11 ± 0.01	0.17 ± 0.01	0.18 ± 0.01	0.17 ± 0.01	0.32 ± 0.03	0.37 ± 0.02
35	0.052 ± 0.004	0.17 ± 0.01	0.27 ± 0.01	0.26 ± 0.01	0.27 ± 0.01	0.35 ± 0.04	0.52 ± 0.04
40	0.067 ± 0.005	0.24 ± 0.02	0.43 ± 0.02	0.42 ± 0.02	0.49 ± 0.01	0.44 ± 0.02	0.65 ± 0.04
E_{act} [kcal mol^{-1}]	15.6 ± 3	15 ± 1	17.3 ± 0.3	16 ± 1	20 ± 2	6.1 ± 0.1	11 ± 1

Minimal values of k_a^{in} were observed for the $(AB)_n$ filament, i.e. for the hybridization-driven polymerization, with values even 10-fold lower than those obtained by base-stacking interactions. By changing the number and spatial distribution of the helices involved in the hybridization process, we observed that the initial rate of the reaction scales with the multivalency and accessibility of the binding sites, with the latter playing a dominant role (Figure S21). Moreover, for random oligomers, stacking of monomers at the A tips was about 2- to 3-fold slower than stacking of monomers at the B tips (Figure 3c). These findings are in good agreement with the FRET and AFM data obtained for dimer formation (Figures 2 and S4 and S5) and match with the higher energy barrier of AA stacking (15 ± 1 kcal mol^{-1}) as compared to BB stacking (6.1 ± 0.1 kcal mol^{-1}) (Figure 3d). Similar conclusions apply to stacking of dimers into oligomers. Interestingly, formation of the $(BAAB)_n$ filament upon stacking at the BB interface showed a rapid increase in the FRET signal followed by a monotonic decrease after only 30 min, particularly at high monomer concentrations (Figure S20). This strengthens the hypothesis that a limited shape-complementarity of DNA origami units facilitates association, however, at the expenses of a less stable bond, eventually preventing the formation of long polymers. Along the same reasoning, the rate of random filament formation is expected to be initially dominated by a fast BB stacking, with the

https://doi.org/10.1021/acs.nanolett.2c02255
Nano Lett. 2022, 22, 8818−8826

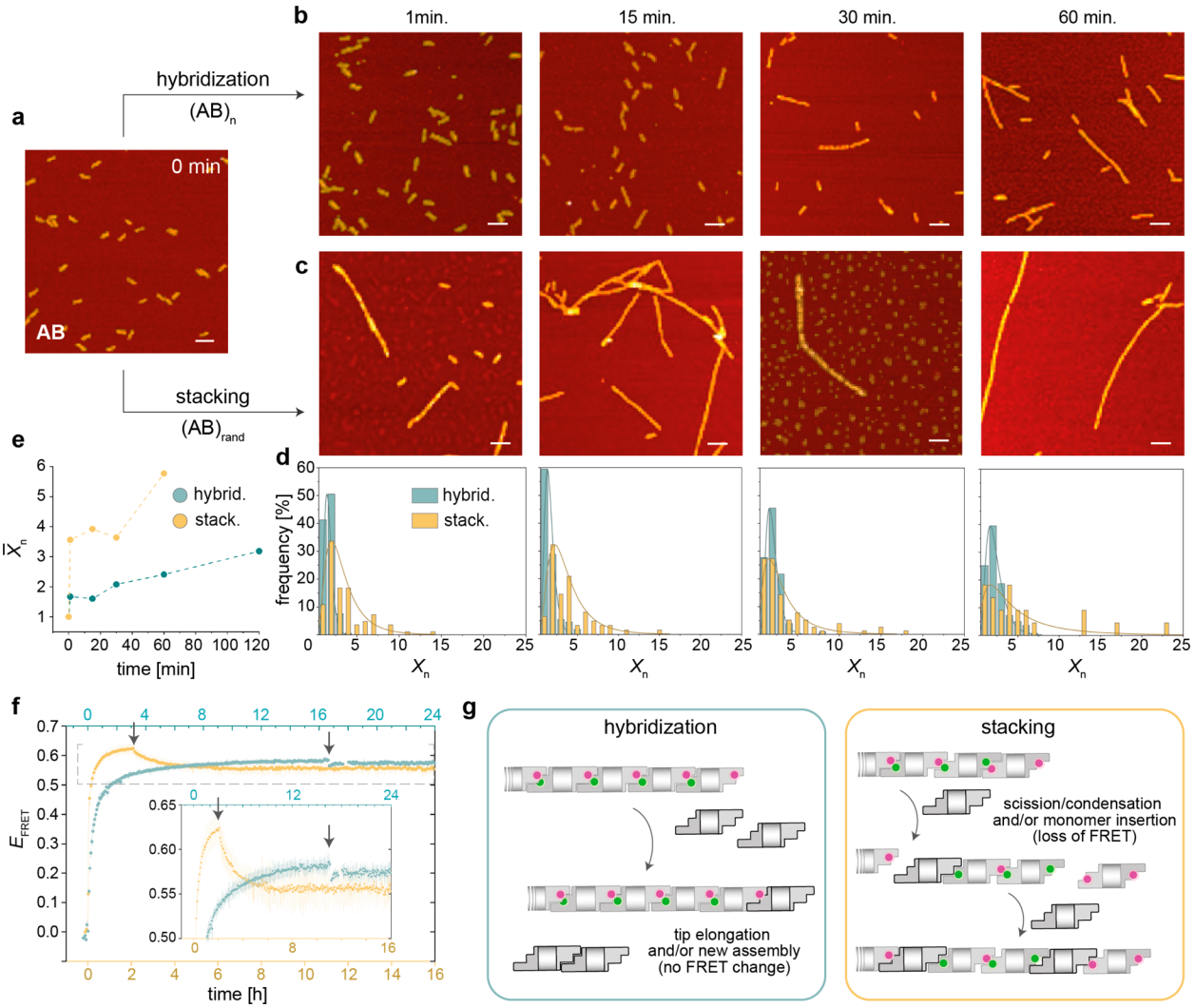

Figure 4. Kinetics of DNA origami filament growth (II). Upon addition of activation strands to a solution of inactive monomer (a), AFM imaging of the reaction mixture was performed at increasing time-points to monitor the formation of hybridized (b) or stacked (c) filaments. Scale bars are 200 nm. (d) Number chain-length distributions at different time-points (X_n is the degree of polymerization, defined as the number of linked monomers). (e) Plots of the number-average polymerization degree ($\bar{X}_n$) over time. (f) A solution of fluorescently labeled $(AB)_n$ or $(AB)_{rand}$ filament at equilibrium (green and yellow curves, respectively) was treated with an equimolar amount of unlabeled monomer (at the time-point indicated by the arrows), and the change in the FRET signal was recorded over time. Whereas the hybridized filament did not show any appreciable FRET change, the stacked filament adapted to the perturbation by decreasing its FRET efficiency by about 10%. (g) Schematic representation of the proposed polymer growth events: the hybridization-driven assembly of the DNA origami monomer mostly proceeds through tip elongation or formation of newly formed short oligomers (left panel); stacking-driven assembly instead preferentially occurs through fragmentation/condensation events that may favor the insertion of monomers into pre-existing oligomers (right panel). Only one pair of FRET labels is used here for clarity (cfr. Figure 1d).

equilibrium state dictated by the statistical distribution of all possible contributions to stacking (AB, AA and BB). Therefore, for a random filament at equilibrium, the fraction of each stacking mode should be proportional to the number of shape-complementary patches needed for its stabilization, with AB > AA > BB (corresponding to 24, 16, and 8 pairs of stacked helices). This is the trend we observed by TEM imaging of individual random filaments marked at the A tip with two gold nanoparticles (Figure S22 and SI Note 3).

Although our FRET assays are well suited to monitor monomer association, they cannot reliably distinguish many small filaments from few larger ones and are therefore not indicative of the average size of the polymers. We therefore monitored the $(AB)_n$ and $(AB)_{rand}$ filaments by AFM in air at different time points (Figure 4). Though surface-related effects may lead to data that do not reflect the situation in solution, previous studies on this design[36] have shown that chain lengths can be reliably measured in the initial phase of the reaction, i.e. when polymers are still relatively short (<2 μm). Random stacking of monomers led to formation of μm-long filaments already after 1 min incubation (X_n up to 10), whereas comparable lengths were reached by the hybridized $(AB)_n$ chain only upon 30 min (Figure 4a–c and Figure S23). After 1 h reaction, hybridized polymers still contain about 20% monomers and short oligomers (2 to 4 monomers), while a small fraction of randomly stacked polymers become longer than 2 μm (X_n > 20), with about 15–20% unreacted monomers and short oligomers still present in solution (Figure 4d). The change in the number-average polymerization degree ($\bar{X}_n$) over time confirmed that the rate of DNA origami

https://doi.org/10.1021/acs.nanolett.2c02255
Nano Lett. 2022, 22, 8818–8826

filament formation depends on the type of interaction used to connect the monomers together, with stacking being significantly faster than hybridization and nonlinearly dependent on time (Figure 4e). Interestingly, in both polymerization processes, the monomer is not the most abundant species in the number chain-length distributions[50] and is almost completely consumed upon long equilibration times (Figure S24). This is unexpected for an ideal step-growth polymerization and might be due to the formation of kinetically trapped species, favored by the high number of interactions between monomers and/or fragments and low off-rates.

To better visualize the different dynamics of the polymers, we monitored the change in FRET signal upon addition of unlabeled monomer to a solution of fluorescently labeled $(AB)_n$ or $(AB)_{rand}$ filaments at equilibrium (green and yellow curves in Figure 4f). The hybridized filament showed almost no change in FRET signal, suggesting that addition of monomers mostly occurs at the tips of preformed filaments or results in the formation of new oligomers (Figure 4g, left panel). Conversely, a 10% decrease in FRET was observed for the randomly stacked filament, indicating the occurrence of more frequent fragmentation/condensation events that may favor the insertion of monomers into pre-existing filaments (Figure 4g, right panel). This hypothesis was confirmed by real-time AFM imaging of the polymerization process in liquid phase (SI Videos 1 and 2). We hypothesize that immediately upon addition of activation strands, the unpaired regions of the scaffold at the monomer tips become hybridized. This is true for both the hybridized and stacked polymers and cannot contribute to their difference in growth rate. However, for the hybridized polymer to form, the staples bound to each monomer tip need to displace their counterparts from the scaffold of the adjacent monomer, which may reasonably take longer than simple stacking of blunt ends (Figure S25).

Altogether, these findings provide deeper insights into the time-course polymerization of DNA origami monomers by multivalent hybridization or stacking interactions and indicate the limitations of an ideal step-growth model to describe these processes. Finally, our data reveal energetic features of monomer association that remain typically undisclosed when observing the reaction at equilibrium conditions. The energetic differences between hybridized and stacked monomers are indeed minimal once the filaments are formed, as demonstrated by the rather similar thermal profiles of exemplary FRET-labeled filaments (Figures S26 and S27).

CONCLUSION

Controlling the kinetics of DNA filament formation is a challenging goal, mostly addressed until now using small DNA tiles. Conversely, less has been done to master the assembly/disassembly of DNA origami filaments, although recent studies have demonstrated the feasibility of this idea and its potential implementations in nanomaterial science.[38] We here show that hybridization interactions, being directional, guide the ordered arrangement of the monomers, however at the expenses of a slower association rate. Base-stacking interactions instead are faster but nondirectional and must be carefully designed to guide the assembly process. We show that the insertion of helical gaps at the interface of stacked monomers can be used to modulate the association rate and the thermal stability of the resulting polymer. In conclusion, our work contributes to the fundamental understanding of hierarchical DNA origami assembly and shows how this process can be fine-tuned by intervention at the unit-to-unit interface and, most importantly, in a modular fashion, that is, using the same ditopic unit to activate different assembly paths. This strategy can be not only applied to obtain a predefined equilibrium state but also to manipulate the kinetic route to it, providing a valuable tool for the development of advanced DNA-based materials.

ASSOCIATED CONTENT

Supporting Information

SI Video 1: ABn_hybridization.avi SI Video 2: AB_rand_-stacking.avi The Supporting Information is available free of charge at https://pubs.acs.org/doi/10.1021/acs.nanolett.2c02255.

Sample preparation and experimental setups, isothermal-FRET curves, temperature-dependent FRET curves, agarose gel electrophoresis and TEM characterizations, kinetic analysis of isothermal FRET profiles, analysis of thermal hysteresis, supporting figures and DNA sequences (PDF)

Real-time AFM imaging of the polymerization process in liquid phase (AVI)

Real-time AFM imaging of the polymerization process in liquid phase (AVI)

AUTHOR INFORMATION

Corresponding Author

Barbara Saccà − *Center of Medical Biotechnology (ZMB) and Center for Nanointegration Duisburg-Essen (CENIDE), University Duisburg-Essen, 45141 Essen, Germany;* orcid.org/0000-0003-2708-2272; Email: barbara.sacca@uni-due.de

Author

Lena J. Stenke − *Center of Medical Biotechnology (ZMB) and Center for Nanointegration Duisburg-Essen (CENIDE), University Duisburg-Essen, 45141 Essen, Germany*

Complete contact information is available at: https://pubs.acs.org/10.1021/acs.nanolett.2c02255

Author Contributions

The manuscript was written through contributions of all authors. All authors have given approval to the final version of the manuscript.

Notes

The authors declare no competing financial interest.

ACKNOWLEDGMENTS

The project has been realized with financial support from the DFG (CRC 1093, project A6 to B.S. and large instrumentation program INST 20876/336-1 FUGG to B.S.). We are thankful to Dr. Wolfgang G. Pfeifer (The Ohio State University, U.S.A.) for initial support in DNA design, as well as to Dr. Michael Erkelenz and Dr. Andreas Jaekel (University of Duisburg-Essen) for assistance in the synthesis of gold nanoparticles and TEM imaging of NP-modified DNA origami.

REFERENCES

(1) Revenu, C.; Athman, R.; Robine, S.; Louvard, D. The Co-Workers of Actin Filaments: From Cell Structures to Signals. *Nat. Rev. Mol. Cell Biol.* **2004**, *5*, 635.

(2) Herrmann, H.; Bär, H.; Kreplak, L.; Strelkov, S. V.; Aebi, U. Intermediate Filaments: From Cell Architecture to Nanomechanics. *Nat. Rev. Mol. Cell Biol.* **2007**, *8*, 562.
(3) Borisy, G.; Heald, R.; Howard, J.; Janke, C.; Musacchio, A.; Nogales, E. Microtubules: 50 Years on from the Discovery of Tubulin. *Nat. Rev. Mol. Cell Biol.* **2016**, *17*, 322.
(4) Fletcher, D. A.; Mullins, R. D. Cell Mechanics and the Cytoskeleton. *Nature* **2010**, *463*, 485−492.
(5) Akhmanova, A.; Steinmetz, M. O. Control of Microtubule Organization and Dynamics: Two Ends in the Limelight. *Nat. Rev. Mol. Cell Biol.* **2015**, *16*, 711.
(6) Bezanilla, M.; Gladfelter, A. S.; Kovar, D. R.; Lee, W. L. Cytoskeletal Dynamics: A View from the Membrane. *J. Cell Biol.* **2015**, *209*, 329−337.
(7) Oosawa, F.; Kasai, M. A Theory of Linear and Helical Aggregations of Macromolecules. *J. Mol. Biol.* **1962**, *4*, 10−21.
(8) Goldstein, R. F.; Stryer, L. Cooperative Polymerization Reactions. Analytical Approximations, Numerical Examples, and Experimental Strategy. *Biophys. J.* **1986**, *50*, 583−599.
(9) Morris, A. M.; Watzky, M. A.; Finke, R. G. Protein Aggregation Kinetics, Mechanism, and Curve-Fitting: A Review of the Literature. *Biochim. Biophys. Acta* **2009**, *1794*, 375−397.
(10) De Greef, T. F.; Smulders, M. M.; Wolffs, M.; Schenning, A. P.; Sijbesma, R. P.; Meijer, E. W. Supramolecular Polymerization. *Chem. Rev.* **2009**, *109*, 5687−5754.
(11) Aida, T.; Meijer, E. W.; Stupp, S. I. Functional Supramolecular Polymers. *Science* **2012**, *335*, 813−817.
(12) de Greef, T. F.; Meijer, E. W. Materials Science: Supramolecular Polymers. *Nature* **2008**, *453*, 171−173.
(13) Brunsveld, L.; Folmer, B. J.; Meijer, E. W.; Sijbesma, R. P. Supramolecular Polymers. *Chem. Rev.* **2001**, *101*, 4071−4098.
(14) Kang, J.; Miyajima, D.; Mori, T.; Inoue, Y.; Itoh, Y.; Aida, T. Noncovalent Assembly. A Rational Strategy for the Realization of Chain-Growth Supramolecular Polymerization. *Science* **2015**, *347*, 646−651.
(15) Korevaar, P. A.; George, S. J.; Markvoort, A. J.; Smulders, M. M.; Hilbers, P. A.; Schenning, A. P.; De Greef, T. F.; Meijer, E. W. Pathway Complexity in Supramolecular Polymerization. *Nature* **2012**, *481*, 492−496.
(16) Fan, X.; Walther, A. 1d Colloidal Chains: Recent Progress from Formation to Emergent Properties and Applications. *Chem. Soc. Rev.* **2022**, *51*, 4023−4074.
(17) Pfeifer, W.; Saccà, B. Synthetic DNA Filaments: From Design to Applications. *Biol. Chem.* **2018**, *399*, 773−785.
(18) Mathieu, F.; Liao, S.; Kopatsch, J.; Wang, T.; Mao, C.; Seeman, N. C. Six-Helix Bundles Designed from DNA. *Nano Lett.* **2005**, *5*, 661−665.
(19) O'Neill, P.; Rothemund, P. W.; Kumar, A.; Fygenson, D. K. Sturdier DNA Nanotubes Via Ligation. *Nano Lett.* **2006**, *6*, 1379−1383.
(20) Rothemund, P. W.; Ekani-Nkodo, A.; Papadakis, N.; Kumar, A.; Fygenson, D. K.; Winfree, E. Design and Characterization of Programmable DNA Nanotubes. *J. Am. Chem. Soc.* **2004**, *126*, 16344−16352.
(21) Wang, T.; Schiffels, D.; Cuesta, S. M.; Fygenson, D. K.; Seeman, N. C. Design and Characterization of 1d Nanotubes and 2d Periodic Arrays Self-Assembled from DNA Multi-Helix Bundles. *J. Am. Chem. Soc.* **2012**, *134*, 1606−1616.
(22) Yin, P.; Hariadi, R. F.; Sahu, S.; Choi, H. M.; Park, S. H.; Labean, T. H.; Reif, J. H. Programming DNA Tube Circumferences. *Science* **2008**, *321*, 824−826.
(23) Schiffels, D.; Liedl, T.; Fygenson, D. K. Nanoscale Structure and Microscale Stiffness of DNA Nanotubes. *ACS Nano* **2013**, *7*, 6700−6710.
(24) Maier, A. M.; Bae, W.; Schiffels, D.; Emmerig, J. F.; Schiff, M.; Liedl, T. Self-Assembled DNA Tubes Forming Helices of Controlled Diameter and Chirality. *ACS Nano* **2017**, *11*, 1301−1306.
(25) Schulman, R.; Winfree, E. Synthesis of Crystals with a Programmable Kinetic Barrier to Nucleation. *Proc. Natl. Acad. Sci. U.S.A.* **2007**, *104*, 15236−15241.
(26) Evans, C. G.; Hariadi, R. F.; Winfree, E. Direct Atomic Force Microscopy Observation of DNA Tile Crystal Growth at the Single-Molecule Level. *J. Am. Chem. Soc.* **2012**, *134*, 10485−10492.
(27) Schulman, R.; Yurke, B.; Winfree, E. Robust Self-Replication of Combinatorial Information Via Crystal Growth and Scission. *Proc. Natl. Acad. Sci. U. S. A.* **2012**, *109*, 6405−6410.
(28) Schaffter, S. W.; Scalise, D.; Murphy, T. M.; Patel, A.; Schulman, R. Feedback Regulation of Crystal Growth by Buffering Monomer Concentration. *Nat. Commun.* **2020**, *11*, 6057.
(29) Li, W.; Yang, Y.; Jiang, S.; Yan, H.; Liu, Y. Controlled Nucleation and Growth of DNA Tile Arrays within Prescribed DNA Origami Frames and Their Dynamics. *J. Am. Chem. Soc.* **2014**, *136*, 3724−3727.
(30) Mohammed, A. M.; Sulc, P.; Zenk, J.; Schulman, R. Self-Assembling DNA Nanotubes to Connect Molecular Landmarks. *Nat. Nanotechnol.* **2017**, *12*, 312−316.
(31) Buchberger, A.; Simmons, C. R.; Fahmi, N. E.; Freeman, R.; Stephanopoulos, N. Hierarchical Assembly of Nucleic Acid/Coiled-Coil Peptide Nanostructures. *J. Am. Chem. Soc.* **2020**, *142*, 1406−1416.
(32) Berengut, J. F.; Wong, C. K.; Berengut, J. C.; Doye, J. P. K.; Ouldridge, T. E.; Lee, L. K. Self-Limiting Polymerization of DNA Origami Subunits with Strain Accumulation. *ACS Nano* **2020**, *14*, 17428−17441.
(33) Li, Z.; Liu, M.; Wang, L.; Nangreave, J.; Yan, H.; Liu, Y. Molecular Behavior of DNA Origami in Higher-Order Self-Assembly. *J. Am. Chem. Soc.* **2010**, *132*, 13545−13552.
(34) Gerling, T.; Wagenbauer, K. F.; Neuner, A. M.; Dietz, H. Dynamic DNA Devices and Assemblies Formed by Shape-Complementary, Non-Base Pairing 3d Components. *Science* **2015**, *347*, 1446−1452.
(35) Woo, S.; Rothemund, P. W. Programmable Molecular Recognition Based on the Geometry of DNA Nanostructures. *Nat. Chem.* **2011**, *3*, 620−627.
(36) Pfeifer, W.; Lill, P.; Gatsogiannis, C.; Saccà, B. Hierarchical Assembly of DNA Filaments with Designer Elastic Properties. *ACS Nano* **2018**, *12*, 44−55.
(37) Tigges, T.; Heuser, T.; Tiwari, R.; Walther, A. 3d DNA Origami Cuboids as Monodisperse Patchy Nanoparticles for Switchable Hierarchical Self-Assembly. *Nano Lett.* **2016**, *16*, 7870−7874.
(38) Jungmann, R.; Scheible, M.; Kuzyk, A.; Pardatscher, G.; Castro, C. E.; Simmel, F. C. DNA Origami-Based Nanoribbons: Assembly, Length Distribution, and Twist. *Nanotechnology* **2011**, *22*, 275301.
(39) Groeer, S.; Walther, A. Switchable Supracolloidal 3d DNA Origami Nanotubes Mediated through Fuel/Antifuel Reactions. *Nanoscale* **2020**, *12*, 16995−17004.
(40) Loescher, S.; Walther, A. Supracolloidal Self-Assembly of Divalent Janus 3d DNA Origami Via Programmable Multivalent Host/Guest Interactions. *Angew. Chem., Int. Ed.* **2020**, *59*, 5515−5520.
(41) Franquelim, H. G.; Dietz, H.; Schwille, P. Reversible Membrane Deformations by Straight DNA Origami Filaments. *Soft Matter* **2021**, *17*, 276−287.
(42) Mostarac, D.; Xiong, Y.; Gang, O.; Kantorovich, S. Nanopolymers for Magnetic Applications: How to Choose the Architecture? *Nanoscale* **2022**, *14*, 11139−11151.
(43) Xiong, Y.; Lin, Z.; Mostarac, D.; Minevich, B.; Peng, Q.; Zhu, G.; Sanchez, P. A.; Kantorovich, S.; Ke, Y.; Gang, O. Divalent Multilinking Bonds Control Growth and Morphology of Nanopolymers. *Nano Lett.* **2021**, *21*, 10547−10554.
(44) Rajendran, A.; Endo, M.; Katsuda, Y.; Hidaka, K.; Sugiyama, H. Programmed Two-Dimensional Self-Assembly of Multiple DNA Origami Jigsaw Pieces. *ACS Nano* **2011**, *5*, 665−671.
(45) Pfeifer, W.; Saccà, B. From Nano to Macro through Hierarchical Self-Assembly: The DNA Paradigm. *Chembiochem* **2016**, *17*, 1063−1080.

https://doi.org/10.1021/acs.nanolett.2c02255
Nano Lett. 2022, 22, 8818−8826

(46) Wei, X.; Nangreave, J.; Jiang, S.; Yan, H.; Liu, Y. Mapping the Thermal Behavior of DNA Origami Nanostructures. *J. Am. Chem. Soc.* **2013**, *135*, 6165−6176.
(47) Andrews, B. T.; Capraro, D. T.; Sulkowska, J. I.; Onuchic, J. N.; Jennings, P. A. Hysteresis as a Marker for Complex, Overlapping Landscapes in Proteins. *J. Phys. Chem. Lett.* **2013**, *4*, 180−188.
(48) Yakovchuk, P.; Protozanova, E.; Frank-Kamenetskii, M. D. Base-Stacking and Base-Pairing Contributions into Thermal Stability of the DNA Double Helix. *Nucleic Acids Res.* **2006**, *34*, 564−574.
(49) Guo, H.; Tullius, T. D. Gapped DNA Is Anisotropically Bent. *Proc. Natl. Acad. Sci. U. S. A.* **2003**, *100*, 3743−3747.
(50) Meira, G.; Oliva, H. Molecular Weight Distributions in Ideal Polymerization Reactors: An Introductory Review. *Lat. Am. Appl. Res.* **2011**, *41*, 389−401.

https://doi.org/10.1021/acs.nanolett.2c02255
Nano Lett. 2022, 22, 8818−8826